Renewable Energy 75 (2015) 626–639

Contents lists available at ScienceDirect

Renewable Energy

journal homepage: www.elsevier.com/locate/renene

Effect of waves on the tidal energy resource at a planned tidal stream array

M. Reza Hashemi*, Simon P. Neill, Peter E. Robins, Alan G. Davies, Matt J. Lewis

School of Ocean Sciences, Bangor University, Menai Bridge, UK

ARTICLE INFO

Article history:
Received 3 June 2014
Accepted 6 October 2014
Available online 3 November 2014

Keywords:
Wave–current interaction
Resource assessment
TELEMAC
SWAN
NW European shelf
Irish Sea

ABSTRACT

Wave–current interaction (WCI) processes can potentially alter tidal currents, and consequently affect the tidal stream resource at wave exposed sites. In this research, a high resolution coupled wave-tide model of a proposed tidal stream array has been developed. We investigated the effect of WCI processes on the tidal resource of the site for typical dominant wave scenarios of the region. We have implemented a simplified method to include the effect of waves on bottom friction. The results show that as a consequence of the combined effects of the wave radiation stresses and enhanced bottom friction, the tidal energy resource can be reduced by up to 20% and 15%, for extreme and mean winter wave scenarios, respectively. Whilst this study assessed the impact for a site relatively exposed to waves, the magnitude of this effect is variable depending on the wave climate of a region, and is expected to be different, particularly, in sites which are more exposed to waves. Such effects can be investigated in detail in future studies using a similar procedure to that presented here. It was also shown that the wind generated currents due to wind shear stress can alter the distribution of this effect.

1. Introduction

The NW European shelf seas are amongst several regions in the world where relatively strong waves are present at many locations that are potentially suitable for the development of tidal stream arrays [1]. Waves can have a critical effect on planning, operation, maintenance, and generally, assessment of the interactions of a tidal energy converter (TEC) device with the marine environment. For instance, wave-induced loads have an important role in the TEC design process [2]. Additionally, wave–current interaction processes affect the turbulence, and the dynamics of sediment transport [3]; therefore, they should be considered when the impact of a TEC device, or an array of such devices, on the environment is studied.

Wave effects can be investigated on various forms of ocean currents – which are driven by forces generated by wind, air pressure, heating and cooling, Coriolis, and astronomical tidal currents; however, tidal-stream sites are usually located in shallow regions of shelf seas which are vertically well mixed and dominated by tidal forcing [4]. Further, the development of tidal-stream sites is primarily based on tidally generated currents. Therefore, the interaction of astronomical tidal currents and waves is of primary importance at tidal-stream sites, in this respect.

Ocean models are widely used to characterise the tidal energy resources of potential tidal-stream sites (e.g. Refs. [5–7]), in conjunction with direct measurement of currents. While these models can simulate tidal currents using relatively established procedures, simulating the effect of waves on tidal currents usually requires additional modelling steps, including the development of a wave model, and a coupling procedure. Apart from a few studies [1,6,8,9], the interaction of waves and tidal currents has not generally been considered in the assessment of marine renewable energy resources (e.g. Refs. [10–12,7]). In particular, much more effort has been invested in characterising the effect of tides on the wave energy resource [1,6,8], in comparison with quantifying the effect of waves on the tidal energy resource. Nevertheless, previous research has shown that wave–current interaction processes can change the hydrodynamics of tidal currents via several mechanisms such as wave induced forces and enhanced bottom friction (e.g. Refs. [13–15]), which could considerably alter the tidal energy resource of a site. These effects can be significant for water depths less than 50 m [16], where the majority of first generation tidal devices are likely to operate [17].

The theory of wave effects on currents has been extensively developed in previous research, and can be implemented using a range of coupled Ocean-Wave-Sediment Transport models [18,19].

* Corresponding author.
E-mail address: r.hashemi@bangor.ac.uk (M.R. Hashemi).

http://dx.doi.org/10.1016/j.renene.2014.10.029

However, few studies have attempted to simulate the interaction of tides and waves over the northwest European shelf seas [20,21]. For instance, Bolanos-Sanchez et al. [22] and Bolanos et al. [23] coupled the POLCOMS (Proudman Oceanographic Laboratory Coastal Ocean Modelling System) ocean model and the WAM (WAve Model), and implemented several wave–current interaction processes, including wave refraction by currents, bottom friction, enhanced wind drag due to waves, Stokes drift, wave radiation stresses, and Doppler velocity. The POLCOMS-WAM coupled modelling system has been applied in a number of research studies, such as surge prediction in the Irish Sea [24].

Among coupled modelling systems which can simulate the interaction of tidal currents and waves, TELEMAC is an open access code which is used frequently for tidal energy resource assessment, both for academic research and commercial projects [25,11,26,27]. The TELEMAC numerical discretisation is based on the unstructured finite element/volume method, and allows the user to refine the mesh in regions of interest, without encountering complications which arise from the nesting procedure. In addition to hydrodynamic modules, TELEMAC has a spectral wave module, TOMAWAC (TELEMAC-based Operational Model Addressing Wave Action Computation), which can simulate the evolution of waves on a mesh which is common to all modules, and export the wave parameters to the current model for the inclusion of wave–current interaction processes [28]. TELEMAC has been previously used to model complex coastal regions where wave-tide interaction plays a key role in sediment transport [29].

In this research, the effect of waves on the tidal energy resource at a proposed tidal stream array has been investigated. The site is within the coastal waters of Anglesey, North Wales, which is one of the hot spots for tidal stream development, and is likely to be the site of one of the first commercial tidal arrays in UK waters.

Section 2 introduces the study region, sources of data, and numerical models used in this study. In particular, the details of the methodology which have been implemented to study the effect of waves on the tidal energy resource is discussed in Section 2.5. All symbols used to describe model formulations or wave current interaction formulae are listed in Table 1. The results are presented in Section 3, which demonstrate the effect of waves on the tidal energy resource in various forms: wave forces, enhanced bottom friction, and combined effects. Section 4 provides additional discussion on the effect of wind generated currents, and highlights topics for further research (e.g. 3-D effects). Finally, our conclusions are summarised in Section 5.

Table 1
List of symbols.

Symbol	Description
A	Semi orbital wave excursion, $A = U_w T_w/2\pi$.
C	Chezy coefficient, $C = \sqrt{(g/C_d)}$.
C^*	Enhanced Chezy coefficient due to WCI near the bed.
C_D	Drag coefficient.
C_D^*	Enhanced drag coefficient due to WCI near the bed.
C_g	Wave group velocity, $½(1 + 2kh/\sinh 2kh)$.
d	Grain diameter ($d = d_{50}$, median grain size).
E	Spectral energy density function $E = E(\sigma,\theta)$.
f_w	Wave friction factor, $f_w = 0.237(A/k_s)^{-0.52}$ [3].
F_x,F_y	Wave induced forces; $F = \sqrt{F_x^2 + F_y^2}$.
h	Water depth.
H_s	Significant wave height.
I	Percentage effect of WCI on current power over a tidal period.
k	Wave number.
k_s	Nikuradse bed roughness.
k_a	Apparent (enhanced) bed roughness due to WCI.
M	Number of data points for computing the mean absolute error.
n	Ratio of the wave group velocity to the wave celerity, C_g/C.
N	Wave action density function.
p	Water pressure.
$\overline{P}$	Average tidal power.
$\mathbf{Q}$	Various source and sink terms in the wave conservation energy.
S_h	Source or sink of mass in continuity equation.
S_i	Source or sink of momentum in i direction (x or y).
S_{xx}	Component of the radiation stress tensor, evaluated by: $\int\int \frac{E}{2}\left[2n(\cos\theta)^2 + (2n-1)\right] d\sigma d\theta$.
S_{yy}	Component of the radiation stress tensor, evaluated by: $\int\int \frac{E}{2}[2n(\sin\theta)^2 + (2n-1)] d\sigma d\theta$.
S_{xy}	Component of the radiation stress tensor, evaluated by: $S_{xy} = S_{yx} = \int\int En\sin\theta\cos\theta d\sigma d\theta$.
T_w	Wave period.
T_{sn}	Spring neap cycle period, about 14.765 days.
u_c	Depth-averaged current velocity.; $u_c = \lvert\mathbf{u}\rvert$.
u_c^*	Depth-averaged current velocity affected by wave–current interaction.
U_w	Near bed wave induced orbital velocity.
z_s	Free surface elevation.
$\mathbf{u}$	Depth averaged current velocity vector.
γ	A coefficient used to compute apparent bed roughness; $\gamma = 0.80 + \varphi - 0.3\varphi^2$.
θ	Angle of propagation for waves.
λ	Ratio of the pure wave to pure current bed shear stresses.
ξ	Ratio of the enhanced drag coefficient to drag coefficient.
σ	Wave angular frequency, $\sigma = 2\pi/T_w$.
τ_c	Current induced bed shear stress.
τ_w	Wave induced bed shear stress.
τ_m	Mean combined wave–current induced bed shear stress.
φ	Angle between wave direction and current direction.

2. Methods

2.1. Study region

The Irish Sea is a highly energetic shelf sea region, with high tidal velocities generated where flow is constricted around headlands [30]. One such example is the northwestern headland of Anglesey (Fig. 1a), a large island located off the NW coast of Wales, where tidal flow is constricted by a bathymetric feature called the Skerries and hence further accelerated.

Due to proximity of the Skerries site to a good grid connection and Holyhead port, suitable bathymetry and peak spring tidal currents in excess of 2.5 m/s [25], Marine Current Turbines (MCT)/Siemens has proposed to install a tidal stream array off the NW coast of Anglesey. The array site is a sound between the Isle of Anglesey and a small group of islands known as the Skerries, less than 1 km from the coast. The proposed tidal stream array consists of five SeaGen S 2 MW tidal stream turbines, with a total array capacity of around 10 MW (www.marineturbines.com). More information on the device can be found at the MCT and SeaGen websites (www.seageneration.co.uk). Apart from this site, a Crown Estate tidal energy demonstration zone has been planned to the west of Holy Island which is close to this site. Other tidal energy companies are also looking for suitable sites in this region for tidal energy development.

2.2. Description of models

Although a number of models have been developed for this region (e.g. Refs. [31,12]), these studies have focused mainly on tides or sediment transport [25]. Wave characteristics at potential tidal stream sites should be considered in several respects, such as wave induced hydrodynamic loading, operation and maintenance, wave-tide interactions, and sediment transport. Accordingly, a coupled tide-wave model of the region, which includes the effect of waves on currents and vice versa, was developed using the TELEMAC modelling system [32].

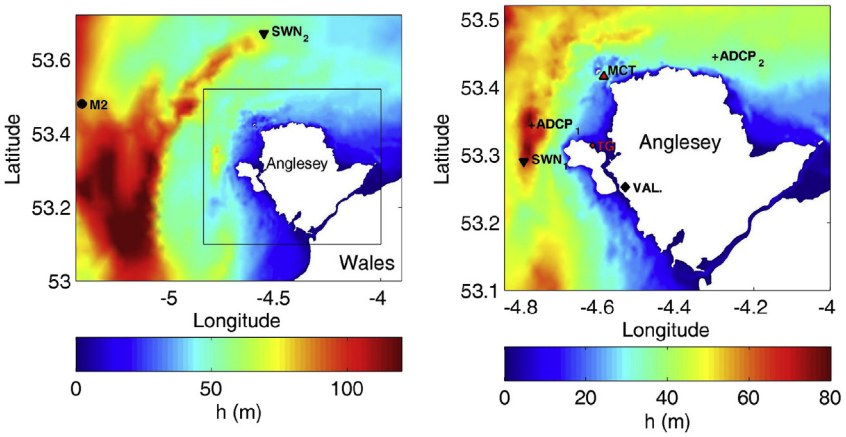

(a) Location map and bathymetry (m)

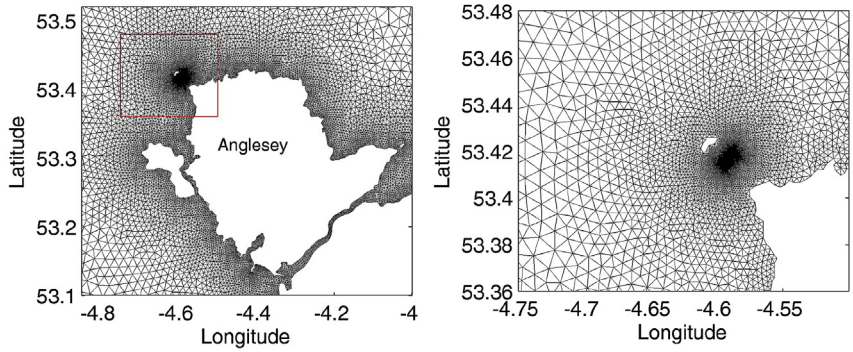

(b) Finite Element Mesh (Magnified view)

Fig. 1. Study area, bathymetry, and a view of the unstructured mesh (part of the computational domain) used to discretise the domain. (a) also shows the locations of several points of interest as follows, MCT: Planned tidal stream array at the Skerries, Anglesey; TG: Holyhead tidal gauge station; ACDP: ADCP deployment; VAL.: Valley Met Office Station; M2: M2 Wave buoy; SWN_1, SWN_2: SWAN model output points.

2.2.1. TELEMAC modelling system

TELEMAC is a finite element or finite volume modelling system which was originally developed to simulate free surface flow. The theoretical/numerical formulation of TELEMAC is described in Hervouet [33], and its source codes and manuals are available online: www.telemacsystem.com. TELEMAC comprises a suite of modules for the simulation of hydrodynamic and morphodynamic processes in oceanic/coastal environments including shallow water (horizontal) flows (TELEMAC-2D), 3-D flows (TELEMAC-3D), sediment transport and bed evolution (SISYPHE), and waves (TOMAWAC). Villaret et al. [28] recently presented several validation test cases of TELEMAC which involved various modules. In the latest version of TELEMAC (i.e. v6.3), the hydrodynamic (TELEMAC-2D), wave, and sediment transport modules are coupled: the modules exchange data at a user defined time step. More details about wave–current interaction simulation using TELEMAC is provided in Section 2.5. TELEMAC-2D, which has been used in this study, is based on the depth-averaged Navier Stokes Equations:

$$\frac{\partial h}{\partial t} + \mathbf{u}\cdot\nabla(h) + h\nabla\cdot\mathbf{u} = S_h \tag{1}$$

$$\frac{\partial u_i}{\partial t} + \mathbf{u}\cdot\nabla(u_i) = -g\frac{\partial z_s}{\partial x_i} + S_{u_i} + \frac{1}{h}\nabla\cdot(h\nu_t\nabla u_i), i = x,\ y \tag{2}$$

where h is the water depth, S_h represent sources/sinks of mass in the continuity equation, $\mathbf{u}$ is the depth averaged velocity, ν_t is the momentum diffusion coefficient (turbulence and dispersion), z_s is the water elevation, S_{ui} represent other forces (friction, wave forces, wind stress, etc.), and i represents either x or y directions. TELEMAC benefits from an unstructured mesh, which allows the use of very high resolution mesh at locations of interest without resort to nesting. The model was used to characterise the tide and wave conditions in and around the Skerries.

TOMAWAC, the wave module of TELEMAC, is a third generation wave model which solves the evolution of the directional spectrum of the wave action. In realistic sea states, the wave energy is distributed over a range of frequencies and directions. The spectral energy density function is the intensity of the wave energy per unit frequency, per unit direction ($E = E(\sigma,\theta)$; see Table 1 for definition of symbols), and can represent the wave sea state at a particular time and location. In spectral models like TOMAWAC or SWAN, 'wave action density', rather than wave spectral density, is used as the state variable, since it is conserved in presence of ambient currents [34,35]. The wave action is defined as: $N(\vec{x}, \vec{k}, t) = E/(\rho g\sigma)$, and is conserved as follows.

$$\frac{\partial N}{\partial t} + (\mathbf{c_g} + \mathbf{u})\cdot\nabla_{\vec{x},\vec{k}}(N) = \mathbf{Q} \tag{3}$$

where $\mathbf{c_g} = (c_g k_x/k, c_g k_y/k)$, and $\mathbf{Q}$ represents various source and sink terms. TOMAWAC includes deep and shallow water physics such as refraction, white-capping, bottom friction and depth-induced wave breaking, as well as non-linear wave–wave quadruplet and triad interactions. TOMAWAC can be applied to a range of scales from continental shelf seas to coastal zones [34].

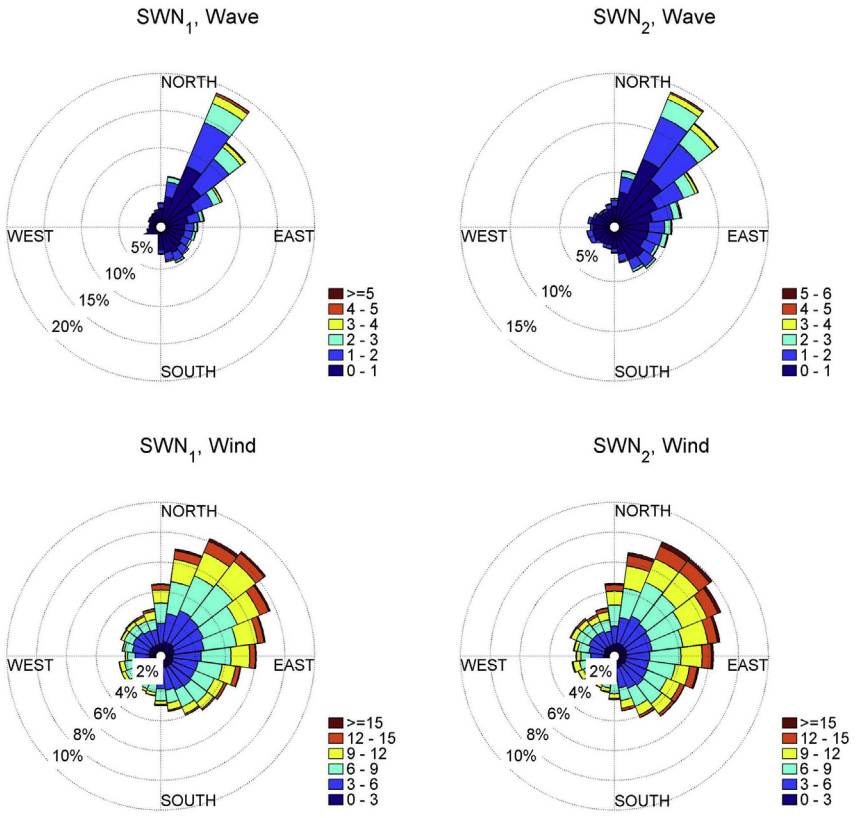

Fig. 2. Wave and wind roses for two locations (SWN_1 & SWN_2) near the tidal stream site (See Fig. 1a). The results are based on 10 years (2003–2012) of SWAN simulation for the NW European shelf seas. The colour scales for the waves and wind roses are significant wave height (m) and wind speed (m/s), respectively. (For interpretation of the references to colour in this figure legend, the reader is referred to the web version of this article.)

2.2.2. TELEMAC settings

An unstructured mesh of the region was created with variable resolution, being relatively fine (15–250 m) around the site and Anglesey, and coarser (500–2000 m) elsewhere in the Irish Sea (Fig. 1b). The model domain covers the whole Irish Sea, extending from 8◦ W to 2.5˚ W, and from 50˚ N to 56˚ N, which is necessary for wave modelling in order to generate sufficient fetch. Gridded Admiralty bathymetry data available at 200 m resolution (digimap.edina.ac.uk) was mapped on to the mesh. TELEMAC2D, the 2-D hydrodynamic module of TELEMAC, solves the 2-D shallow water equations using finite element method to simulate tidal currents, which is a good approximation for the fully mixed barotropic flows in this area. Tidal currents in the NW European shelf seas are dominated by M_2 and S_2: principal lunar and solar semidiurnal components, respectively [36]. The next three tidal constituents, which are relatively significant in some areas of the NW European shelf seas, are K_1 and O_1 lunar diurnal components, and the lunar elliptic semidiurnal constituent, N_2 [37]. Therefore, the open boundaries of the tidal model were forced by 5 tidal constituents (M_2, S_2, N_2, K_1, O_1) interpolated from FES2004 tidal data [37]. For friction, a constant Chezy's coefficient of 70 (approximately equivalent to $C_D = 0.0025$) was used, which led to convincing validation for water level and current speed for the astronomical tides at observation locations. The friction coefficient was then enhanced based on the wave parameters for WCI effects (Section 2.5.2).

TOMAWAC was applied to the same mesh and bathymetry as the TELEMAC2D model. Hourly wind forcing data was provided by the UK Met Office Integrated Data Archive System (MIDAS; for Valley station see Fig. 1). TOMAWAC was run in third-generation mode, including Janssen's wind generation (WAM cycle 4), whitecapping, and quadruplet wave–wave interactions. The bottom friction and depth induced wave breaking were also included in the numerical simulations.

2.2.3. SWAN wave model

Since the high resolution coupled TELEMAC model was expensive to run for long periods of time, a SWAN (Simulating WAves Nearshore) model of the NW European Shelf seas was used to characterise the temporal variability of the wave climate over a decade of simulation. The SWAN model was developed and validated extensively in a previous research study [38].

SWAN is another open source third-generation numerical wave model which simulates random waves from deep waters to the surf zone and coastal regions in the spectral domain. SWAN has been described in Booij et al. [35] and is based on the Eulerian formulation of the discrete spectral balance of action density. It has been widely used for simulating waves at various scales (e.g. Refs. [38,39]). It accounts for refractive propagation over arbitrary bathymetry and ambient current fields. The physics and formulation of SWAN are similar to those of TOMAWAC described in Section 2.2.1; however, in SWAN, the wave action is formulated as a function of wave frequency and direction rather than wave number (used in TOMAWAC). Several processes including wind generation, whitecapping, quadruplet wave–wave interactions, and bottom dissipation are represented explicitly in SWAN.

2.2.4. SWAN settings

The SWAN wave model setting and its validation, which was applied for a decade (2003–2012) of simulation, are described in

detail in Neill and Hashemi [38]. It consisted of a parent model which included the entire North Atlantic at a grid resolution of 1/6° × 1/6°, extending from 60° W to 15° E, and from 40° N to 70° N. 2-D wave spectra were output hourly from the parent model and interpolated to the boundary of an inner nested model of the NW European shelf seas. The inner nested model had a grid resolution of 1/24°×1/24°, extending from 14° W to 11° E, and from 42° N to 62° N. Wind forcing was provided by European Centre for Medium-Range Weather Forecasts (ECMWF; www.ecmwf.int). ERA (European Research Area) Interim reanalysis full resolution data, which are available 3-hourly at a spatial resolution of 3/4°×3/4° were used. SWAN was run in third-generation mode, with Komen linear wave growth, white-capping, and quadruplet wave–wave interactions.

2.3. Wave climate of the region

In contrast to the astronomical tides, the wave climate of a region is highly variable. It has been previously shown that the wave climate of the NW European shelf seas is strongly related to the North Atlantic Oscillation, which has high inter-annual variability [38]. Fig. 2 shows the wave and wind roses at two points (Fig. 1a) off the NW of Anglesey based on the 10 year SWAN simulation. As this figure shows, the strongest and most frequent winds and waves are southwesterly. It is also clear that the probability of waves with significant wave height (H_s) greater than 5 m, or wind speeds in excess of 15 m/s, is quite low. Fig. 3b shows the variability of extreme significant wave heights during winter months to the west of Anglesey over the decade of simulation (Point SWN_1, Fig. 1). According to this figure, the probability of waves with H_s exceeding 5.5 m is very low. Further, January 2005 and December 2007 are the most extreme months in our record, with maximum significant wave heights of 6.7 m and 6.8 m, respectively. The expected (i.e. average) value of an extreme significant wave height during the winter period is 3.9 m. In terms of mean wave conditions (Fig. 3a), January is the most energetic month in this region, with expected significant wave heights of approximately 1.6 m (on average). Based on these wave statistics, the TOMAWAC model was forced with different southwesterly wind scenarios; wind speeds of 10 m/s and 15 m/s seemed appropriate to capture mean and extreme wave scenarios, with significant wave heights of 4.0 m and 1.8 m, respectively at SWN_1 (Fig. 1). In the next sections, TELEMAC2D and TOMAWAC are first validated, and then used to study the effect of waves on tidal energy resources of the site for these scenarios.

2.4. Model validation

The tidal model was validated at several tidal gauge stations within the Irish Sea. The validation results relatively near to the site is presented here. ADCP (acoustic Doppler current profiler) data collected during August 2013, at Holyhead Deep ($ADCP_1$, Fig. 1a), and February 2014, off the northern coast of Anglesey ($ADCP_2$, Fig. 1a), were used for current validation. Fig. 4a shows the comparison of model outputs and observed data at Holyhead tidal gauge. Table 2 also shows the performance of the model for water elevation and current velocity. The mean absolute error, which is reported in Table 2, is defined as.

$$\mathrm{MAE} = \frac{1}{M}\sum_{i=1}^{M}\left|u_c^o(i) - u_c^m(i)\right| \tag{4}$$

where M is the number of data points, u_c^o and u_c^m are observed and predicted values of depth averaged velocities, respectively. The current ellipses for M_2 and S_2 based on the model results and observations have also been compared in Fig. 4b. The model error for M_2 and S_2 amplitudes were 5 cm and 8 cm, and for phases were 2° and 1°, respectively. For $ADCP_1$, the errors of the current ellipse axes directions were 7° and 8° for M_2 and S_2 while less than 2% for magnitudes of the ellipses major axis. The small error in tidal ellipse directions may be associated with the 3-D nature of the flow [40] at this location, which is deeper than the surrounding areas. Similar discrepancies for current velocities have been reported in a previous study of the region which used ADCIRC depth averaged model [12]. Similar results can be seen for $ADCP_2$. The mean absolute error of current velocity for two measurement locations is less than 0.20 m/s. Overall, given the magnitudes of the errors, model performance for both tidal elevations and currents is convincing.

The theoretical average tidal stream energy per unit area (i.e., $\overline{P} = 1/2T_{sn}\int \rho\left|u_c\right|^3 \mathrm{d}t$) over a spring-neap cycle has been plotted in Fig. 5. As this figure shows, the Skerries and west coast of Holyhead are hot spots for tidal energy in northwest Wales. The peak tidal

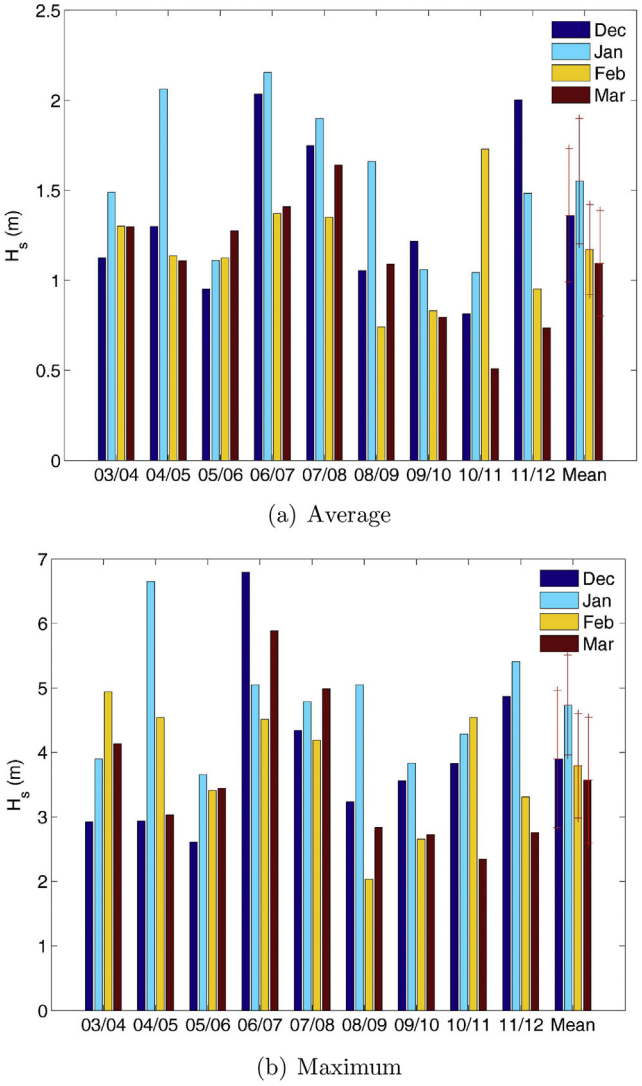

Fig. 3. Distribution of the average and maximum significant wave height at point SWN_1 (See Fig. 1a) over a decade (2003–2012) of simulation. January 2005, and December 2007 are the most extreme months with 6.7 m and 6.8 m significant wave heights, respectively. According to error-bars, which are based on 95% CI, the probability of these events is less than 5%.

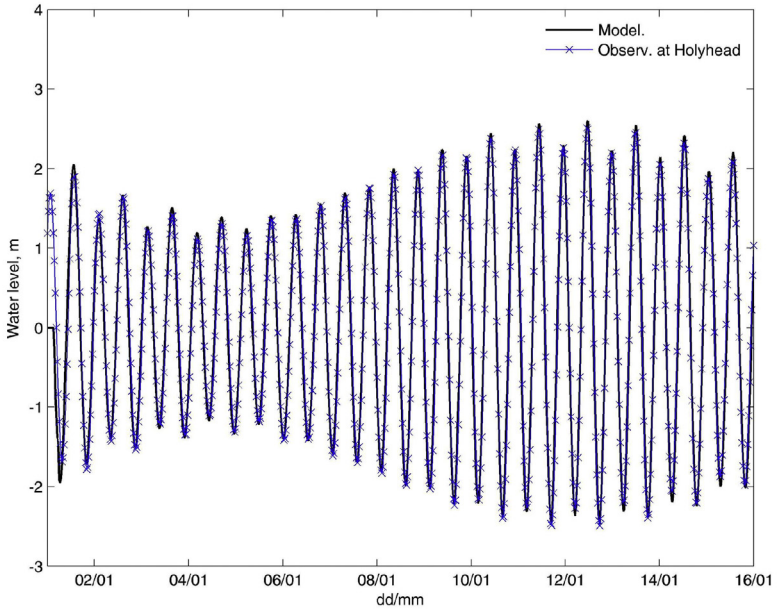

(a) Astronomical tide at Holyhead during 1-16 January 2005.

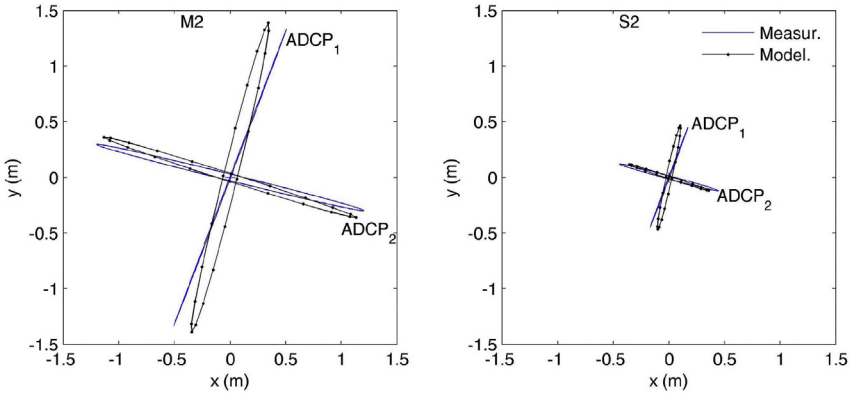

(b) Current ellipses (left M_2 and right S_2) at ADCP points (Fig. 1a)

Fig. 4. Sample validation of the tidal model for elevation and current velocity. See Table 2 for error magnitudes.

current velocity exceeds 3 m/s in parts of this region, and there is a relatively large area where peak tidal velocities exceed 2 m/s.

The TOMAWAC model of the region was validated for January 2005, which represents one of the most extreme months during our analysed period (Fig. 3). Within this month, periods of high, low and average wave condition existed, which provides a highly variable basis for testing the model. Fig. 6 shows the validation of significant wave height and wave period at the M2 wave buoy (Fig. 1), which is the closest available wave buoy to the site. The mean absolute errors for wave height and period are 0.38 m and 0.65 s, respectively, which is within an acceptable range of accuracy, compared with other models of this region (e.g. Ref. [38]). In particular, the model was able to capture the peak wave height on the eighth of January, which is important in the extreme wave scenario.

2.5. Formulation of wave effects on currents

Two important wave effects on currents are: wave induced momentum (or wave radiation stresses), and the enhancement of

Table 2
Performance of the tidal model (in terms of absolute error) for tidal elevation and velocity at a tidal gauge and 2 ADCP measurement points (see Fig. 1 for locations). The mean absolute error is presented for u_c. The variables in this table are defined as follows: a_h and a_h, tidal elevation amplitude and phase, respectively; C_{max} and C_α, current ellipse major axes magnitude and direction, respectively; u_c is the depth averaged velocity.

Variable		Error		
		TG		
M_2	a_h	5 cm		
	ϕ_h	2°	ACDP$_1$	ADCP$_2$
	C_{max}		0.02 m/s	0.04 m/s
	C_α		7°	4°
S_2	a_h	8 cm		
	ϕ_h	1°	ACDP$_1$	ADCP$_2$
	C_{max}		0.02 m/s	0.09 m/s
	C_α		8°	3°
u_c			0.20 m/s	0.14 m/s

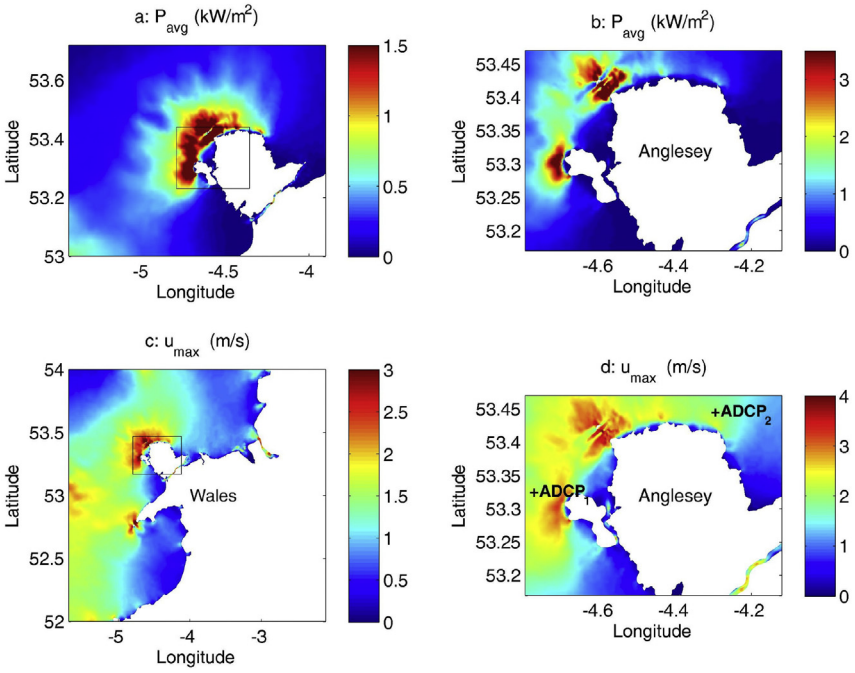

Fig. 5. Simulated mean theoretical tidal stream power (P_{avg}) and peak tidal current velocity (u_{max}) over a spring-neap cycle. The ACDP deployment points are also shown for comparison.

the bottom friction felt by currents due to the interaction with the wave boundary layer. Both effects can be included in coupled wave-tide models by exporting the appropriate wave parameters to the tidal model, and modifying the corresponding parameters in the momentum equation. The effect of these processes on tidal energy is evaluated here by running the tidal model with and without WCI, and then computing the average tidal power. The relative difference, or the effect of a process, was computed using.

$$I = 100 \times \frac{\int \rho \left|u_c^*\right|^3 \mathrm{d}t - \int \rho \left|u_c\right|^3 \mathrm{d}t}{\int \rho \left|u_c^*\right|^3 \mathrm{d}t} \tag{5}$$

where u_c^* is the tidal current affected by a wave–current interaction process, I is the percentage effect, and ρ is the water density. In a coupled TELEMAC2D-TOMAWAC model, the wave radiation forces

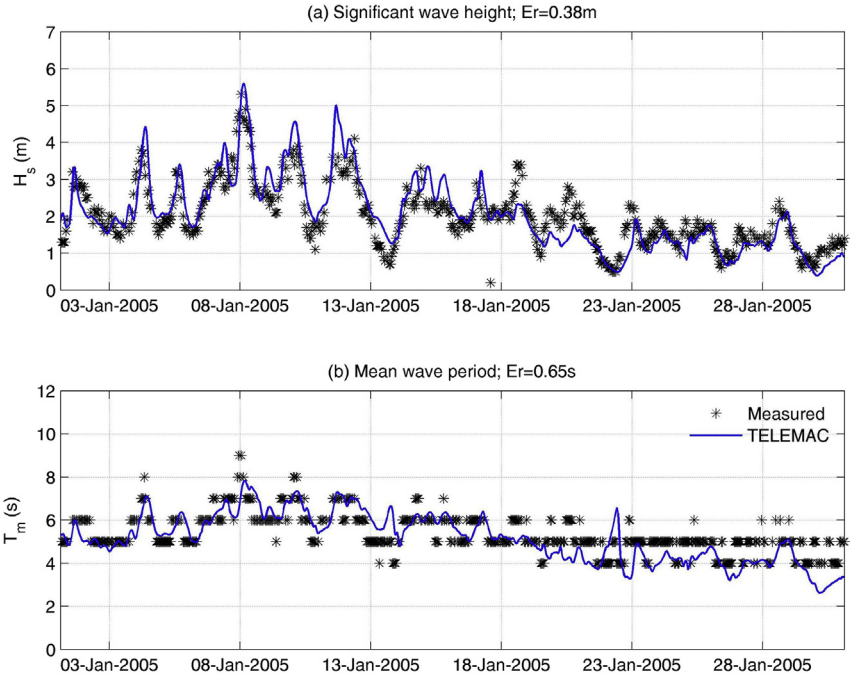

Fig. 6. Comparison of high resolution TOMAWAC results with observed data at M2 wave buoy (See Fig. 1a) during January 2005. The observed mean wave periods have a resolution of 1 s, while model results show more temporal fluctuations.

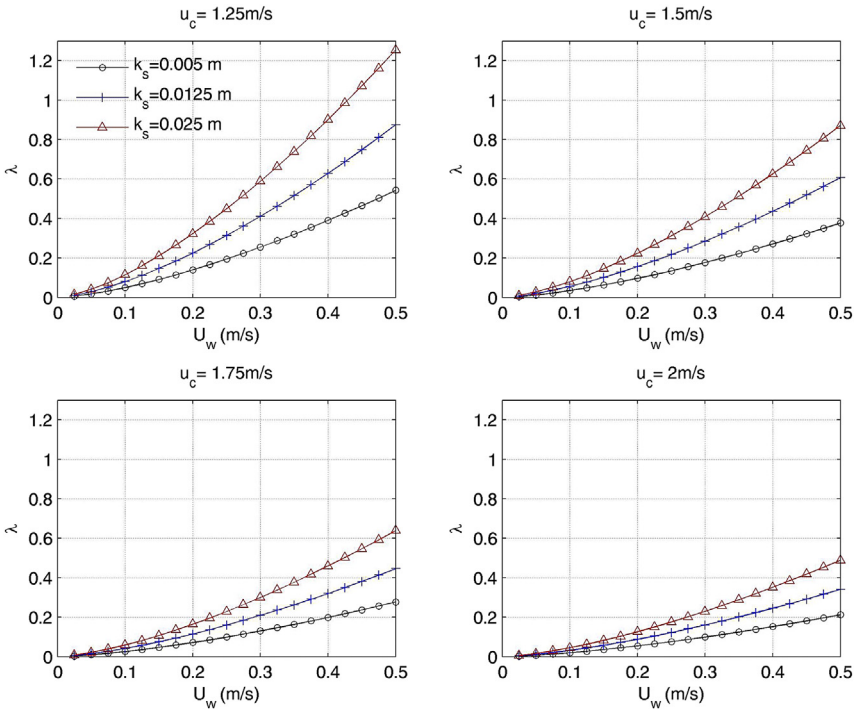

Fig. 7. Ratio of the pure wave to the pure current stresses (λ) for different wave and current conditions.

are automatically computed and fed back to the hydrodynamic model [41]. Further, although the effect of wave induced bed shear stresses are incorporated in the sediment transport module [42], the enhanced bottom friction due to WCI is not included in the hydrodynamic model (i.e. TELEMAC2D) formulations [41]. However, it is possible in the TELEMAC modelling system to modify the subroutines associated with bottom friction and include this process according to the wave parameters (Section 2.5.2).

2.5.1. Wave radiation stresses

Wave radiation stresses are the excess flow of momentum due to the presence of waves [43]. The wave induced forces are computed based on the gradient of the wave radiation stresses as follows [44],

$$F_x = -\left(\frac{\partial S_{xx}}{\partial x} + \frac{\partial S_{xy}}{\partial y}\right); \quad F_y = -\left(\frac{\partial S_{yy}}{\partial y} + \frac{\partial S_{yx}}{\partial x}\right) \tag{6}$$

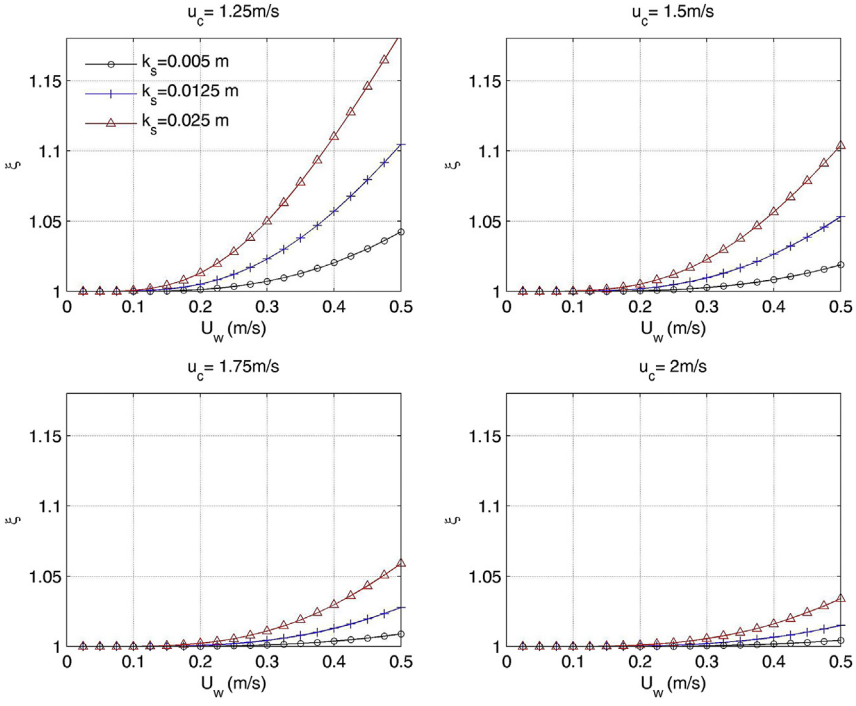

Fig. 8. Enhancement of the bottom drag coefficient due to WCI for a range of tidal currents. ξ is the ratio of the enhanced drag coefficient to the 'pure current' drag coefficient.

where F represents the wave force per unit surface area, and the wave radiation stresses (i.e., S_{ij}) have been defined in Table 1. By analogy, pressure forces are another form of body force, which are stresses generated by the gradient of the water pressure (i.e., $\partial p/\partial x = \rho g \partial h/\partial x$). In general, wave forces are dominant in the near-shore zone, where the gradients of the radiation stresses are high, and can explain wave set-up and longshore currents. In addition, they can potentially change the current velocity in a tidal stream site, especially if there is a dominant wave climate, and this can consequently affect the tidal energy resource.

2.5.2. Enhanced bottom friction

The interaction of waves with the current boundary layer leads to near-bed turbulence, and consequently the bed shear stress. This effect can reduce tidal currents, and since tidal power is proportional to velocity cubed, it can potentially decrease the tidal energy resource at a site. For instance, Wolf and Prandle [13], observed that the amplitudes of tidal currents reduce due to WCI. The WCI effect on the bottom boundary layer has been extensively studied in previous research (e.g. see Refs. [15,14,45,46]). Here, we investigate the sensitivity of bottom friction to this effect, and its implications in tidal energy resource assessment.

In general, ocean hydrodynamic models, like TELEMAC, have several options available to quantify bottom friction [32,47]. Therefore, to empirically account for enhanced friction due to WCI, the bed roughness length corresponding to the Nikuradse law of friction, the bottom drag coefficient corresponding to quadratic friction law, or Chezy coefficient corresponding to the Chezy law, can be modified. For instance, Van Rijn [45] introduced the following relation to enhance the bed roughness in the presence of waves.

$$k_a = k_s \exp\left(\gamma \frac{U_w}{u_c}\right) < 10, \quad \gamma = 0.80 + \varphi - 0.3\varphi^2 \tag{7}$$

where k_a and k_s represent the apparent and physical roughness, respectively; φ is the angle between wave direction and current direction in radians. In practice, the apparent bed roughness due to WCI can be an order of magnitude greater than the physical bed roughness. Alternatively, we applied the concept of mean (over the wave period) drag coefficient due to combined waves and current to increase bottom friction in the present research. The mean bed shear stress due to the combined action of waves and currents is given by Refs. [46,3],

$$\tau_m = \tau_c \left[1 + 1.2\left(\frac{\tau_w}{\tau_c + \tau_w}\right)^{3.2}\right] \tag{8}$$

where τ_c and τ_w are bed shear stresses due to current alone or wave alone, respectively. The bed shear stresses are related to depth averaged current velocity through the drag coefficient,

$$\tau_c = \rho C_D u_c^2, \ \tau_m = \rho C_D^* u_c^2 \tag{9}$$

where C_D and C_D^* are the drag coefficients in the absence and presence of waves, respectively; therefore, Eq. (8) can be written as,

$$\xi = \frac{C_D^*}{C_D} = \left[1 + 1.2\left(\frac{\lambda}{1+\lambda}\right)^{3.2}\right] < 2.2, \quad \lambda = \frac{\tau_w}{\tau_c} \tag{10}$$

Eq. (10) gives the ratio of the combined wave–current drag coefficient to the pure current drag coefficient (i.e. ξ) as a function of the ratio of the wave induced shear stress to the current induced bed shear stress (i.e. λ). The wave induced bed shear stress is a function of the bottom wave orbital velocities (U_w), and can be computed using the wave parameters output from a wave model as follows [3],

$$\tau_w = \frac{1}{2} f_w U_w^2, \quad f_w = 0.237\left(\frac{A}{k_s}\right)^{-0.52} \tag{11}$$

where f_w is the wave friction factor, k_s is Nikuradse bed roughness, and A is the semi orbital wave excursion (see Table 1). Given the dominant wave climate of a region, Eq. (10) (or alternatively Eq. (7)) can be implemented as a simple procedure to assess the effect of waves on the tidal energy resource in terms of enhanced bottom friction. Although more complex and computationally expensive methods are available in 3-D coupled wave-tide models like COAWST (Coupled Ocean Atmosphere Wave Sediment Transport [9,48]), we used this method which is more convenient and significantly less expensive. It is worth mentioning that other friction factors like the Chezy coefficient can be modified using ξ. Since $C = g/C_D^2$, the modified Chezy coefficient will be: $C^* = C/\sqrt{\xi}$.

Figs. 7 and 8 show the enhancement of the bottom drag coefficient due to WCI as a function of the wave induced orbital velocity for several wave and current scenarios. The sensitivity analysis has been carried out for the usual operational condition of a tidal stream site with currents of greater than 1.0 m/s (lower cut-in speed of TECs). In terms of the bed friction, k_s values of 0.005, 0.0125, and 0.025 correspond to seabed sediment grain sizes of 2 mm, 5 mm, and 10 mm, respectively (assuming $k_s = 2.5d_{50}$), values that are typically observed at high energy sites [25].

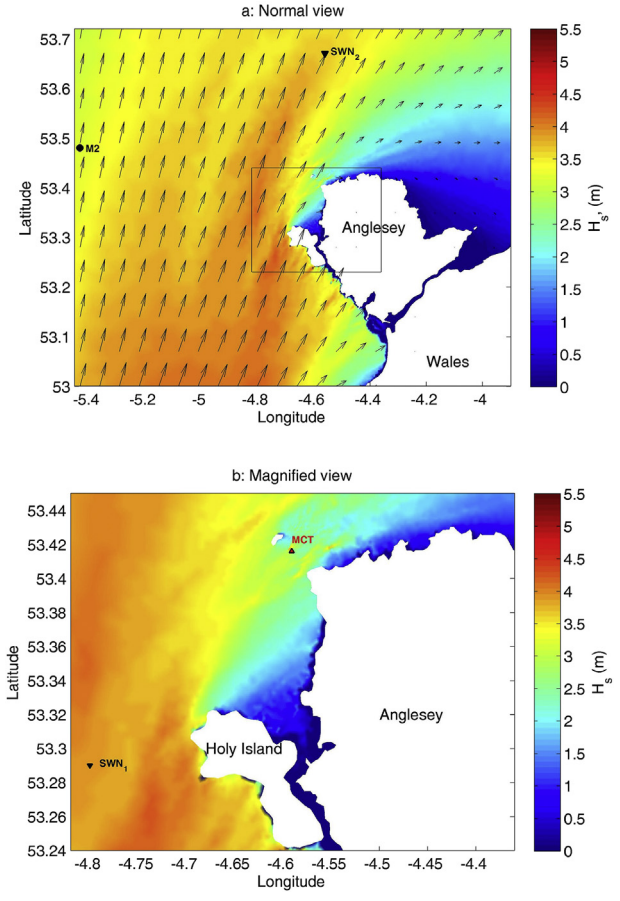

Fig. 9. Spatial distribution of the significant wave height (H_s) for a hypothetical scenario of a southwesterly 15 m/s wind. The colour scales are H_s in m. (For interpretation of the references to colour in this figure legend, the reader is referred to the web version of this article.)

The wave orbital velocity, estimated near the bed, which is the basis for the above computations can be directly output from a wave model like TOMAWAC. Alternatively, it can be parameterised using the surface wave parameters [49,50] or approximated by linear wave theory.

$$U_w = \frac{\pi H_s}{T_w \sinh(kh)} \tag{12}$$

where the wave number, k is computed using the linear dispersion equation ($\sigma^2 = gk\tanh kh$). In the absence of coupled wave-tide models, the above equation (or similar procedures) along with Fig. 8 give a quick estimate of the enhanced bottom friction, which then can be used to approximately compute the effect of WCI on the tidal energy.

3. Results

Based on the wave statistics of the site (Section 2.3), the TOMAWAC model was forced with different southwesterly wind scenarios in stationary mode; wind speeds of 10 m/s and 15 m/s were selected to capture mean and extreme wave scenarios, respectively. To simulate the effect of waves on tidal currents, TELEMAC was run in fully coupled mode, where two-way feedbacks between the wave and the tide models were implemented.

3.1. Effect of wave forces on tidal energy

The spatial distribution of significant wave height for the extreme wave scenario is plotted in Fig. 9, which indicates a wave height of about 4 m at SWN_1. Further, Holy Island has a significant effect on the wave distribution over the NW part of Anglesey, including the Skerries site, for this scenario. The validated TOMAWAC wave model was then used to study the effect of WCI as an element of the coupled wave-tide model of the region. Fig. 10 shows the computed wave radiation stresses, and the corresponding wave forces for two typical wave scenarios. As this figure shows, apart from nearshore zones, the wave forces are also significant in the Skerries tidal stream site, particularly for the extreme wave scenario. Referring to Eq. (6), the gradient of the wave radiation stresses in this area generates the wave forces. Since wave radiation stresses are proportional to wave energy (see Table 1), the spatial change (i.e. gradient) in the wave height distribution leads to the generation of wave induced forces. Referring to Figs. 9 and 10, as a complex result of changes in the bathymetry and coastline, and Holy Island acting as an obstacle in the wave field, the wave height distribution, and consequently wave radiation stresses have a significant gradient around the Skerries. Fig. 11 shows the mean effect of these forces on tidal energy (in percent) over a tidal cycle. Considering the percentages of the impacts, the wave forces have slightly

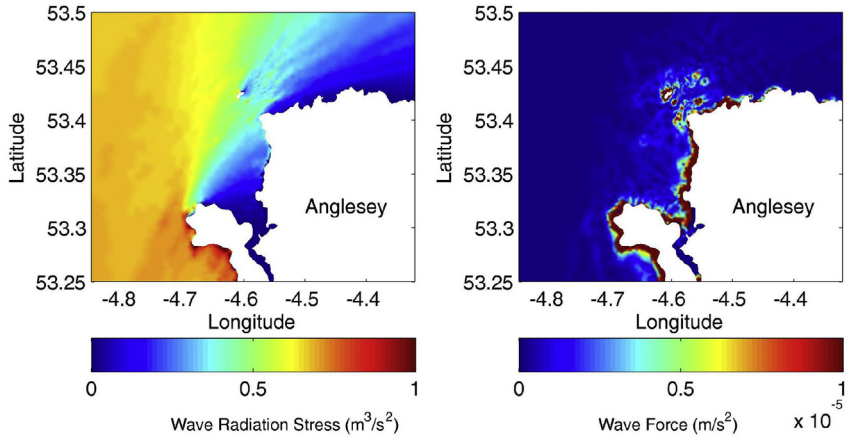

(a) Wave forces for southwesterly wind of 10m/s

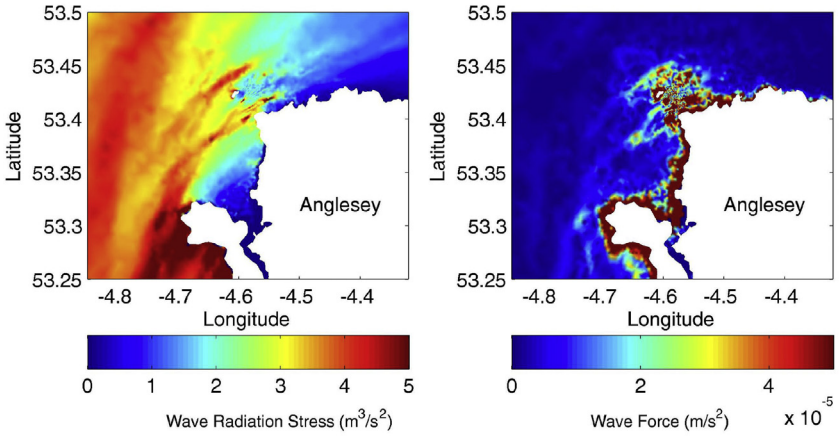

(b) Wave forces for southwesterly wind of 15m/s

Fig. 10. Wave radiation stresses and wave forces (i.e. $F = \sqrt{F_x^2 + F_y^2}$) for two wind scenarios around the Skerries tidal stream site. Wave forces, which are usually expressed in N/m^2, have been normalised by water density and water depth. The wave radiation stresses have been normalised by water density (consistent with the TOMAWAC model outputs).

modified the tidal energy for the average wave scenario (3%), while they have more significant impact for the extreme scenario (7%). Since it is the difference of coupled wave-tide model and decoupled tide model that has been plotted, the effect is an overall reduction of the tidal energy, on average. It is worth mentioning that for the above scenarios, the direction of the wave forces do not change during a tidal cycle, as opposed to tidal currents. Therefore, wave forces, on average, had more effects on opposing currents in contrast to following currents. Nevertheless, the presence of wave forces leads to a new hydrodynamic current field which, in general, is spatially and temporally different from that produced in the absence of waves. Considering the tidal asymmetry of the site [12], further research is needed to study the implication of this asymmetry for tidal energy and sediment transport [51].

3.2. Effect of enhanced bottom friction on tidal energy

To implement the method described in Section 2.5.2, the orbital velocities, and other wave parameters, were computed for the two wave scenarios using TOMAWAC, and used to modify the bottom friction coefficient. The modified bottom friction coefficients were then fed back into the tidal model. This step can either be implemented with a separate code as in this research, or included in the subroutines of TELEMAC. Fig. 12 shows the near-bed wave orbital velocities for the two wave scenarios. As this figure shows, the wave orbital velocities are about 0.30 m/s and 0.08 m/s for the two scenarios, which is equivalent to about a 5% and 1% increase in the bed friction enhancement factor (ξ), respectively (Fig. 8), or lower depending on the current speed and bed roughness. After computing the tidal power based on the modified friction, the effect as a percentage has been plotted in Fig. 13 which is, like the effect of wave forces, significant (6%) for the extreme wave case and very small (2%) for the average wave scenario. Since the effect is always negative (reduction in power), the absolute value has been plotted in this figure.

3.3. Combined effects

In the case of a fully coupled simulation, where wave radiation stresses and enhanced bottom friction are both incorporated in the tidal modelling, the impact of WCI is magnified due to the nonlinear nature of these processes. In other words, due to nonlinearity in the friction and wave induced force terms in the momentum equations, these effects are not simply superimposed. Fig. 14 shows the average effect of both processes on tidal power. As a consequence of WCI, tidal power can decrease by up to 20% and 15%, respectively, for the extreme and average scenarios, which represents a significant effect on the tidal stream resource.

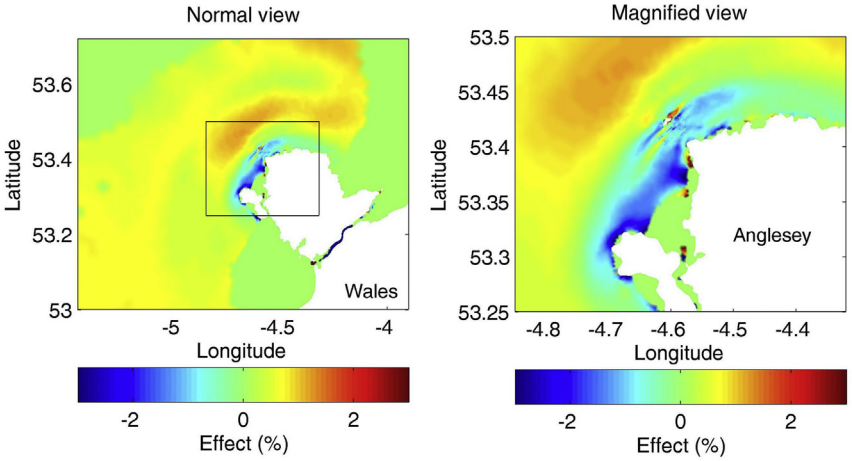

(a) Mean scenario

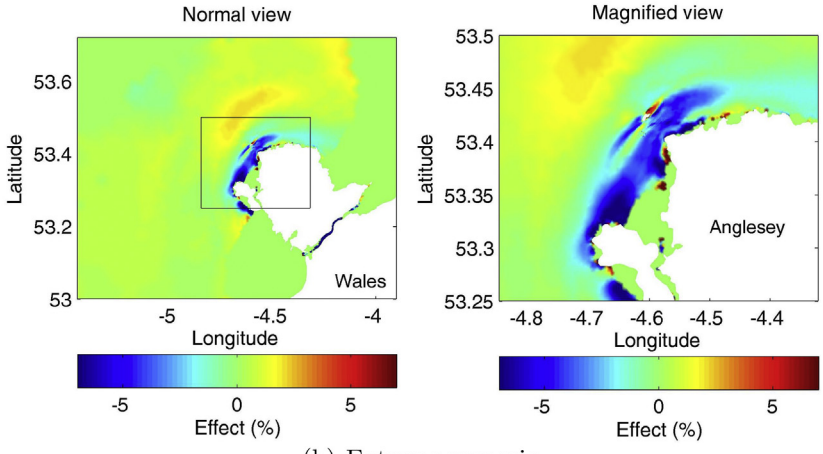

(b) Extreme scenario

Fig. 11. Effect of wave forces on the tidal stream power for two scenarios.

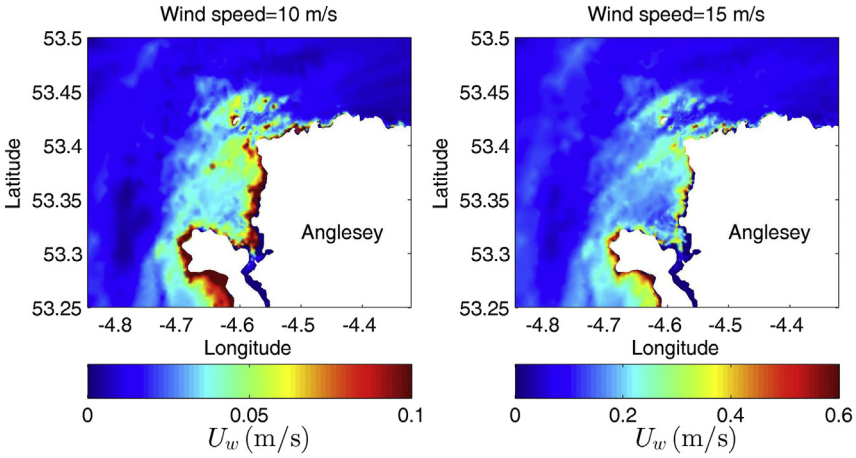

Fig. 12. Wave orbital velocities, U_w (m/s), around the Skerries tidal stream site, assuming two different wave scenarios.

4. Discussion

Another process of interest is wind-driven currents. The effect of wind generated currents can be added to wave effects by including wind shear stresses in the hydrodynamic model (TELEMAC-2D). Fig. 15 shows the results of superimposing the effect of wind generated currents on wave effects for the extreme scenario. As this figure shows, overall, the magnitude of the impact on the tidal energy resource does not change considerably – compared with Fig. 14 – while the distribution changes (reduction) in the vicinity of the tidal-stream site. The depth of penetration of wind generated currents in relation to hub heights of tidal energy devices is another topic of interest, which can be studied using 3-D models. This process can be examined in more detail in future studies. The results are generally in agreement with previous 3-D model studies at tidal energy sites 5.

The Skerries project is likely to be one of the first tidal stream arrays installed in UK waters. The wave climate of this region is moderate, so not as extreme as at other potential tidal stream sites such as NW Scotland, or the west coast of Ireland [38], both coastlines that are directly exposed to North Atlantic waves. Due to the highly non-linear nature of WCI effects, separate studies should be undertaken for other sites, but this research has attempted to provide a simple methodology for a popular hydrodynamic model (TELEMAC) which is used in research, and by developers, for tidal energy studies. It is expected that the effect of WCI processes will be much larger at more exposed tidal stream sites of the NW European shelf seas, but site specific modelling and analysis are required to confirm this and quantify these effects.

Moreover, to protect turbines from extreme wave loads, tidal-stream devices do not operate in extreme wave conditions. Therefore, the effect of waves on the practical tidal energy resource of a region may be unimportant for the extreme scenarios; nevertheless, the effect is still considerable for the average wave scenario, when tidal energy devices still operate. Due to various limitations such as the interactions of tidal devices at array scale, the available extractable tidal energy at a site is usually less than the theoretical tidal energy considered here [52]. The impact of wave-tide interaction on the practical extractable energy resource depends on specific devices and array configurations, and can be investigated as another step. Further, the sensitivity of the tidal resources of a region to bottom friction decreases as a result of substantial drag from a large tidal array [7]. This may reduce the effect of enhanced bottom friction due to waves. The interaction of waves and tidal currents has implications in design, efficiency, and loading of tidal energy devices which is the subject of other research (e.g. Refs. [53–55]).

The analysis which was accomplished in this research was based on depth-averaged quantities. The effect of various WCI processes

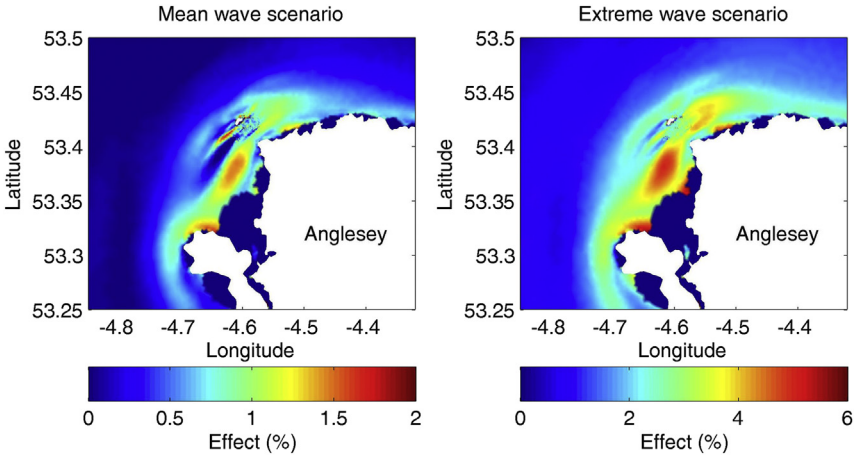

Fig. 13. Effect of enhanced bottom friction due to WCI on tidal stream energy around the Anglesey Skerries site, for two different wave scenarios.

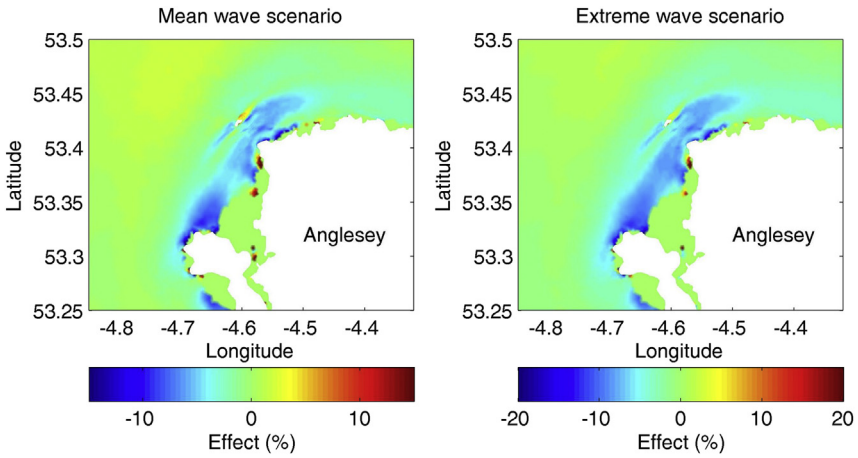

Fig. 14. Combined effect of the enhanced bottom friction (due to WCI) and wave radiation stresses on the tidal stream energy around the Anglesey Skerries site, for two different wave scenarios (15 m/s as the extreme and 10 m/s as the mean scenario).

varies throughout the water column, and given the hub-height of a particular TEC device, it will be useful to assess the vertical variability of these effects using 3-D models [9]. For instance, there is a debate over using depth-averaged radiation-stress gradient as a depth-uniform body force in ocean models [56]. The depth-dependent form of horizontal radiation stress gradient terms has also been proposed [57] and applied in 3-D models [48]. Other aspects such as tidal asymmetry and turbulence can be also addressed in future research [5].

Finally, although Eqs (7) and (8) are based on extensive observations made in previous studies, and it is current practice in ocean models to use similar relations to include wave–current interaction processes, the simultaneous measurement of tidal currents and waves at proposed tidal stream arrays can provide more insight into WCI related issues. Traditionally, deployment of wave buoys in regions of strong tidal currents is more challenging, and so wave data tends to be sparse in such regions. Referring to Eq. (5), it is easy to show that $\delta P/P \propto 3 \times \delta u_c/u_c$, where δ is the variation.[1] Therefore, to observe a 6% change in power, one should be able to detect 2% change in the current measurement, which is likely to be about the order of magnitude of the measurement errors.

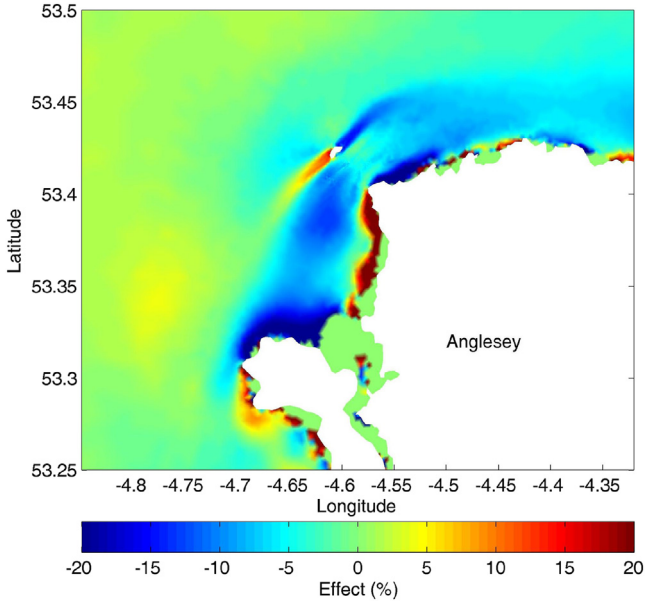

Fig. 15. Combined effect of the enhanced bottom friction (due to WCI), wave radiation stresses, and wind-generated currents on tidal stream power assuming a southwesterly wind of 15 m/s.

5. Conclusions

The effect of WCI processes on the tidal energy resource at the proposed Skerries tidal stream array has been investigated for mean and extreme wave scenarios. In terms of wave radiation stresses, it was shown that both wave forces, and their effect on the tidal energy resource, are significant for the extreme wave scenario, and can reach 7%. A simplified method developed here, which was presented to include the effect of WCI on bottom friction, can be used to assess the sensitivity of the tidal currents and tidal power to these processes, based on the wave climate of a region.

As a result of the combined effects of wave radiation stresses and enhanced bottom friction, the tidal energy resource can be reduced by up to 15% and 20% for mean and extreme winter wave scenarios, respectively, at the Skerries tidal stream site. The impact of these two processes is magnified when they are considered together, rather than separately, due to the nonlinear nature of the forces. For more exposed sites, e.g. NW of Scotland, the impact is expected to be greater. Also, wind generated currents change the distribution of this effect in the vicinity of the tidal-stream site.

The effect of WCI processes on tidal energy increases as the ratio of wave stress to current stress increases. Therefore, this effect is more significant for lower tidal energy sites which are exposed to strong waves, rather than higher tidal energy sites which are exposed to moderate waves.

Simultaneous measurement of waves and tidal currents at potential tidal stream sites is necessary to further investigate the impact of waves on various aspects of tidal energy development. However, it should be stressed that very high accuracy measurements would be required due to relatively small values of WCI processes compared with main parameters of the flow. Nevertheless, the effect of these processes can become significant with respect to other parameters like tidal energy or sediment transport.

[1] $P \propto |u_c|^3$, therefore $\delta P \propto 3|u_c|^2 \delta u_c = 3|u_c|^3 \delta u_c/|u_c|$, which leads to $\delta P \propto 3P\delta u_c/|u_c|$.

Acknowledgements

Thanks to Dr Scott J. Couch of Marine Current Turbine for discussions on the Skerries tidal stream project. The wave buoy data used for model validation was supplied by the Irish Marine Institute and British Oceanographic Data Centre (BODC). The model simulations were made on High Performance Computing (HPC) Wales, a collaboration between Welsh universities, the Welsh Government and Fujitsu. This work was undertaken as part of the SEACAMS project, which is part-funded by the European Union's Convergence European Regional Development Fund, administered by the Welsh Government (Grant number: 80284). Simon Neill and Matt Lewis acknowledge the support of EPSRC SuperGen project EP/J010200/1.

References

[1] Hashemi MR, Neill SP. The role of tides in shelf-scale simulations of the wave energy resource. Renew Energy 2014;69:300–10.
[2] Galloway PW, Myers LE, Bahaj AS. Quantifying wave and yaw effects on a scale tidal stream turbine. Renew Energy 2014;63:297–307.
[3] Soulsby R. Dynamics of marine sands: a manual for practical applications. Thomas Telford; 1997.
[4] Simpson JH, Sharples J. Introduction to the physical and biological oceanography of shelf seas. Cambridge University Press; 2012.
[5] Neill SP, Hashemi MR, Lewis MJ. The role of tidal asymmetry in characterizing the tidal energy resource of Orkney. Renew Energy 2014;68:337–50.
[6] Saruwatari A, Ingram DM, Cradden L. Wave–current interaction effects on marine energy converters. Ocean Eng 2013;73:106–18.
[7] Adcock TAA, Draper S, Houlsby GT, Borthwick AGL, Serhadlıoğlu S. The available power from tidal stream turbines in the pentland firth. Proc R Soc A: Math Phys Eng Sci 2013;469(2157):20130072.
[8] Barbariol F, Benetazzo A, Carniel S, Sclavo M. Improving the assessment of wave energy resources by means of coupled wave-ocean numerical modeling. Renew Energy 2013;60:462–71.
[9] Lewis M, Neill SP, Hashemi MR. Realistic wave conditions and their influence on quantifying the tidal stream energy resource. Appl Energy 2014;136:495–508.
[10] ABPmer. Atlas of UK marine renewable energy resources. Tech. Rep. Department for Business Enterprise & Regulatory Reform; 2008
[11] Blunden LS, Bahaj AS. Initial evaluation of tidal stream energy resources at Portland Bill, UK. Renew Energy 2006;31(2):121–32.
[12] Serhadlıoğlu S, Adcock TAA, Houlsby GT, Draper S, Borthwick AGL. Tidal stream energy resource assessment of the Anglesey Skerries. Int J Mar Energy 2013;3:e98–111.
[13] Wolf J, Prandle D. Some observations of wave–current interaction. Coast Eng 1999;37(3):471–85.
[14] Soulsby RL, Hamm L, Klopman G, Myrhaug D, Simons RR, Thomas GP. Wave-current interaction within and outside the bottom boundary layer. Coast Eng 1993;21(1):41–69.
[15] Davies AG, Soulsby RL, King HL. A numerical model of the combined wave and current bottom boundary layer. J Geophys Res Oceans (1978–2012) 1988;93(C1):491–508.
[16] Prandle D. The influence of bed friction and vertical eddy viscosity on tidal propagation. Cont Shelf Res 1997;17(11):1367–74.
[17] Couch SJ, Bryden I. Tidal current energy extraction: hydrodynamic resource characteristics. Proc Inst Mech Eng Part M: J Eng Marit Environ 2006;220:185–94.
[18] Newberger P, Allen JS. Forcing a three-dimensional, hydrostatic, primitive-equation model for application in the surf zone: 1. formulation. J Geophys Res Oceans 2007;112(C8).
[19] Warner JC, Armstrong B, He R, Zambon JB. Development of a coupled ocean–atmosphere–wave–sediment transport (COAWST) modeling system. Ocean Model 2010;35(3):230–44.
[20] Wolf J. Coastal flooding: impacts of coupled wave–surge–tide models. Nat Hazards 2009;49(2):241–60.
[21] Hashemi MR, Neill SP, Davies AG. A coupled wave-tide model for NW European shelf seas. Geophys Astrophys fluid Dyn 2014. http://dx.doi.org/10.1080/03091929.2014.944909. In press.
[22] Bolanos-Sanchez R, Wolf J, Brown J, Osuna P, Monbaliu J, Sanchez-Arcilla A. Comparison of wave-current interaction formulation using polcoms-wam wave-current model. 2009.
[23] Bolanos R, Osuna P, Wolf J, Monbaliu J, Sanchez-Arcilla A. Development of the POLCOMS–WAM current–wave model. Ocean Model 2011;36(1):102–15.
[24] Brown JM, Souza AJ, Wolf J. An 11-year validation of wave-surge modelling in the Irish Sea, using a nested POLCOMS–WAM modelling system. Ocean Model 2010;33(1):118–28.
[25] Robins PE, Lewis MJ, Neill SP. Impact of tidal-stream arrays in relation to the natural variability of sedimentary processes. Renew Energy 2014;72:311–21.
[26] Burrows R, Walkington I, Yates N, Hedges T, Wolf J, Holt J. The tidal range energy potential of the west coast of the United Kingdom. Appl Ocean Res 2009;31(4):229–38.
[27] Hashemi M, Neill S, Davies A. A numerical study of wave and current fields around Ramsey island tidal energy resource assessment. In: XIXth TELEMAC-MASCARET User Conference. Oxford, United Kingdom; 2012.
[28] Villaret C, Hervouet JM, Kopmann R, Merkel U, Davies AG. Morphodynamic modeling using the Telemac finite-element system. Comput Geosci 2013;53:105–13.
[29] Brown JM, Davies AG. Methods for medium-term prediction of the net sediment transport by waves and currents in complex coastal regions. Cont Shelf Res 2009;29(11):1502–14.
[30] Davies AM, Gerritsen H. An intercomparison of three-dimensional tidal hydrodynamic models of the Irish Sea. Tellus A 1994;46(2):200–21.
[31] Walkington I, Burrows R. Modelling tidal stream power potential. Appl Ocean Res 2009;31(4):239–45.
[32] Hervouet JM. TELEMAC modelling system: an overview. Hydrol Process 2000;14(13):2209–10.
[33] Hervouet JM. Hydrodynamics of free surface flows: modelling with the finite element method. John Wiley & Sons; 2007.
[34] Benoit M, Marcos F, Becq F. Development of a third generation shallow-water wave model with unstructured spatial meshing. Coast Eng Proc 1996;25.
[35] Booij N, Ris R, Holthuijsen LH. A third-generation wave model for coastal regions: 1. Model description and validation. J Geophys Res Oceans 1999;104(C4):7649–66.
[36] Uehara K, Scourse JD, Horsburgh KJ, Lambeck K, Purcell AP. Tidal evolution of the northwest European shelf seas from the last glacial maximum to the present. J Geophys Res Oceans 2006;111(C9).
[37] Lyard F, Lefevre F, Letellier T, Francis O. Modelling the global ocean tides: modern insights from FES2004. Ocean Dyn 2006;56(5–6):394–415.
[38] Neill SP, Hashemi MR. Wave power variability over the northwest European shelf seas. Appl Energy 2013;106:31–46.
[39] Rusu E, Gonçalves M, Guedes Soares C. Evaluation of the wave transformation in an open bay with two spectral models. Ocean Eng 2011;38(16):1763–81.
[40] Stansby PK. Limitations of depth-averaged modeling for shallow wakes. J Hydraulic Eng 2006;132(7):737–40.
[41] Lang P. Telemac-2d user's manual. Tech. Rep. EDF R & D; 2013
[42] Tassi P, Villaret C. Sisyphe v6.3 user's manual. Tech. Rep. EDF R & D; 2014
[43] Longuet-Higgins MS, Stewart R. Radiation stresses in water waves; a physical discussion, with applications. Deep Sea Res Oceanogr Abstr 1964;11:529–62.
[44] Mei CC. The applied dynamics of ocean surface waves. World Sci 1989;1.
[45] Van Rijn LC. Unified view of sediment transport by currents and waves. I: initiation of motion, bed roughness, and bed-load transport. J Hydraulic Eng 2007;133(6):649–67.
[46] Soulsby R, Clarke S. Bed shear-stresses under combined waves and currents on smooth and rough beds. HR Wallingford; 2005. Report TR137.
[47] Shchepetkin AF, McWilliams JC. The regional oceanic modeling system (roms): a split-explicit, free-surface, topography-following-coordinate oceanic model. Ocean Model 2005;9(4):347–404.
[48] Warner JC, Sherwood CR, Signell RP, Harris CK, Arango HG. Development of a three-dimensional, regional, coupled wave, current, and sediment-transport model. Comput Geosci 2008;34(10):1284–306.
[49] Wiberg PL, Sherwood CR. Calculating wave-generated bottom orbital velocities from surface-wave parameters. Comput Geosci 2008;34(10):1243–62.
[50] Soulsby R. Calculating bottom orbital velocity beneath waves. Coast Eng 1987;11(4):371–80.
[51] Neill SP, Jordan JR, Couch SJ. Impact of tidal energy converter (TEC) arrays on the dynamics of headland sand banks. Renew Energy 2012;37(1):387–97.
[52] Garrett C, Cummins P. The power potential of tidal currents in channels. Proc R Soc A: Math Phys Eng Sci 2005;461(2060):2563–72.
[53] Gaurier B, Davies P, Deuff A, Germain G. Flume tank characterization of marine current turbine blade behaviour under current and wave loading. Renew Energy 2013;59:1–12.
[54] Bahaj AS, Batten W, McCann G. Experimental verifications of numerical predictions for the hydrodynamic performance of horizontal axis marine current turbines. Renew Energy 2007;32(15):2479–90.
[55] Clarke JA, Connor G, Grant AD, Johnstone CM. Design and testing of a contra-rotating tidal current turbine. Proc Inst Mech Eng Part A: J Power Energy 2007;221(2):171–9.
[56] Uchiyama Y, McWilliams JC, Shchepetkin AF. Wave–current interaction in an oceanic circulation model with a vortex-force formalism: application to the surf zone. Ocean Model 2010;34(1):16–35.
[57] Xia H, Xia Z, Zhu L. Vertical variation in radiation stress and wave-induced current. Coast Eng 2004;51(4):309–21.